International Journal of Remote Sensing

ISSN: 0143-1161 (Print) 1366-5901 (Online) Journal homepage: www.tandfonline.com/journals/tres20

Coupling remote sensing data with *in-situ* optical measurements to estimate suspended particulate matter under the Evros river influence (North-East Aegean sea, Greece)

Athina Tsapanou, Emmanouil Oikonomou, Panagiotis Drakopoulos, Serafeim Poulos & Georgios Sylaios

To cite this article: Athina Tsapanou, Emmanouil Oikonomou, Panagiotis Drakopoulos, Serafeim Poulos & Georgios Sylaios (2020) Coupling remote sensing data with *in-situ* optical measurements to estimate suspended particulate matter under the Evros river influence (North-East Aegean sea, Greece), International Journal of Remote Sensing, 41:6, 2062-2080, DOI: 10.1080/01431161.2019.1685713

To link to this article: https://doi.org/10.1080/01431161.2019.1685713

Published online: 05 Nov 2019.

INTERNATIONAL JOURNAL OF REMOTE SENSING
2020, VOL. 41, NO. 6, 2062–2080
https://doi.org/10.1080/01431161.2019.1685713

Taylor & Francis
Taylor & Francis Group

Coupling remote sensing data with *in-situ* optical measurements to estimate suspended particulate matter under the Evros river influence (North-East Aegean sea, Greece)

Athina Tsapanou[a], Emmanouil Oikonomou[b], Panagiotis Drakopoulos[c], Serafeim Poulos[a] and Georgios Sylaios[d]

[a]Department of Geology & Geoenvironment, National & Kapodistrian University of Athens, Athens, Greece; [b]Department of Surveying & Geoinformatics Engineering, University of West Attica, Aigaleo, Greece; [c]Laboratory of Optical Metrology, University of West Attica, Aigaleo, Greece; [d]Department of Environmental Engineering, Democritus University of Thrace, Xanthi, Greece

ABSTRACT

Monitoring the riverine output of Suspended Particulate Matter (SPM) distribution in marine embayment is a crucial factor for the water quality of neighbouring coastal regions. This study presents satellite-derived SPM calculations against *in-situ* measurements in the continental shelf of North-East Aegean surrounding the trans-boundary Evros river mouth. Surface SPM, Inherent Optical Properties (IOPs) and remote sensing reflectance (R_{rs}) data were collected in a field campaign during low river discharge period (June 2016). The relationship between the optical backscattering coefficient (b_{bp}) and the *in-situ* SPM concentrations was investigated. Subsequently, an empirical single band model was applied for estimating SPM concentrations by using the Landsat-8 Operational Land Imager (L8/OLI) red band and the model was then locally tuned within the study area. Furthermore, a multi-band SPM-retrieval algorithm was developed using the *in-situ* surface reflectance R_{rs} for calibration and it was validated using the Leave-One-Out Cross Validation technique (LOOCV). The relationship between *in-situ* SPM and backscattering coefficient values showed good proportionality, thus, nominating the predominance of terrestrial mineral particles. Validation against field measurements indicated that the SPM concentrations derived from the newly-developed multi-band algorithm had an improved significance correlation (96%), compared to both the single band model (not-tuned) (coefficient of determination, R^2 = 0.82) and its locally tuned version (R^2 = 0.83). Most importantly, the generated multi-band model apart from exhibiting the best performance (R^2 = 0.93), it revealed high SPM spots which were not detected by the locally tuned single band model, indicating additional processes originating from river outflows, coastal erosion and subaqueous thermal springs in the area. In contrast, the locally tuned single band model overestimated SPM values in offshore waters, where low concentrations are encountered under the influence of the clear Black Sea Water (BSW).

ARTICLE HISTORY
Received 2 October 2018
Accepted 20 September 2019

CONTACT Athina Tsapanou atsapanou@geol.uoa.gr Department of Geology & Geoenvironment, National & Kapodistrian University of Athens, Athens, Greece

1. Introduction

In recent years, research has been motivated by the overall environmental and economic importance for monitoring the Suspended Particulate Matter (SPM) distribution in coastal areas. River systems are the primary supplying source of particulate matter into the ocean water column, with 95% of the runoff sediments leading to shelf sedimentation (Meade 1996). At the special case of transboundary river systems, their management consists of increased complexity in terms of water and sediment quality investigation, since they are shared between interconnected countries (Wiering et al. 2010).

Several efficient SPM retrieval methods were developed by using the remote sensing reflectance, R_{rs} (λ) (in sr^{-1}) (Nechad, Ruddick, and Park 2010; Froidefond et al. 2002), defined as the ratio of the water-leaving spectral radiance to the downwelling spectral irradiance, with both parameters referring to just-above the water surface. R_{rs} (λ) can be observed *in-situ*, with either above or in-water radiance and irradiance measurements; it can also be recorded by satellites for estimating SPM concentrations.

An alternative way to derive information about the suspended marine material is through the inversion relationship between R_{rs} and the inherent optical properties (IOPs), by measuring the optical backscattering coefficient (b_b) in seawater (Alcântara, Curtarelli, and Stech. 2016). Water molecules, salts, organic and inorganic particles, etc., are considered to be the constituents contributing to (b_b) (Stramski et al. 2004).

Satellite observations have been used effectively for monitoring surface SPM and their dynamics (Doxaran et al.2002b; Vantrepotte et al. 2013), with the majority of past studies making initially use of medium resolution sensors (e.g. Moderate Resolution Imaging Spectroradiometer-MODIS), which offered high temporal resolution but lacking in spatial detail. The free-access data of Landsat-8 (L8) at 15–30 m spatial and 16 days temporal resolution, significantly improved the investigation of small-scale spatial variability in oceanographic processes; it has also permitted a long-term analysis (Lymburner et al. 2016) and the study of SPM interannual and seasonal variations and spatial distributions, compared with riverine runoff, sediment discharge, and resuspension processes related to hydrodynamics (Qiu et al. 2017).

The algorithms implemented to estimate SPM values are based on empirical, semi-empirical or theoretical formulas. In particular, numerous empirical algorithms used different spectral band combinations that were implemented in coastal areas of various water turbidity regimes (Doxaran, Froidefond, and Castaing 2002b; Ouillon, Douillet, and Andréfouët 2004; Moore, Aiken, and Lavender 1999; Zhang et al. 2010).

Until recently, the SPM calculation through medium-high resolution sensors was achieved by exploiting marine reflection at a single red channel; Vanhellemont and Ruddick (2014) used L8 images to reveal the impact of offshore wind farms on SPM, by applying a single band red model. In addition, both linear and non-linear (logarithmic) models have been applied to Landsat imagery in order to successfully predict sediment concentrations in aquatic systems (e.g. Wang et al. 2017). The application of several band ratios (Doxaran et al. 2002a; Doxaran, Froidefond, and Castaing 2002b; Qiu 2013; Tassan 1994) or multiband methods (Zhang et al. 2010; Tassan 1994; Siswanto et al. 2011) significantly reduced the atmospheric correction errors of satellite-derived products.

In the available literature is shown that no absolute correspondence exists between the spectrum of the estimated water-column parameters and the satellite spectral reflectance,

thus a theory of its own is not adequate for developing SPM calculation formulas. The existence, however, of multiple and different approaches along with their limitations, it makes it a difficult and challenging issue to select the most appropriate within a defined area of interest. Furthermore, in the empirical methods, the strong dependence between SPM and R_{rs} ranges is an inhibiting factor that requires local calibration of the coefficients in a specific geographical region.

The objectives of this study are: (i) to validate simultaneous above-water ocean colour measurements with SPM field observations and to compare them against concurrent remote sensing data, and (ii) to determine the most appropriate algorithm for predicting SPM concentration from ocean colour and Landsat-8-derived surface reflectance R_{rs}. Firstly, an original approach for SPM estimations from ocean colour is proposed based on *in-situ* backscattering measurements and secondly, a single band model (Nechad, Ruddick, and Park 2010) is tested, then locally tuned and finally compared to a newly generated multi-band model for the area. Moreover, the critical assessment of the cross-correlation between these methodologies aims not only to certify the validity of the derived remotely sensed data, but also to reveal the benefits and drawbacks of each approach.

2. Materials and methods

2.1. The study area

The wider Alexandroupolis Gulf (Figure 1) is part of the inner continental shelf in the NE Aegean Sea (Samothraki Plateau), being characterized by relatively shallow water (<35 m) and a rather smooth morphology. The transboundary Evros river, draining an area of approximately 53.000 km^2, debouches on the eastern coast of the Gulf. Mean annual water river discharge accounts for no more than 250 km^3 (Skoulikidis 2018), while its suspended sediment potential load can reach 8.5×10^6 tones (Milliman and Farnsworth 2011). During the last decades this sediment flux is considered to be drastically reduced (down to 0.5×10^6 ton), due to the presence of more than 30 major dams in its river network (Karditsa and Poulos 2013; Karditsa, Tsapanou, and Poulos 2019).

The North East (NE) Aegean Sea is an essentially tideless environment with astronomical tidal range <10 cm (Tsimplis 1994). Nearshore currents flow westwards during the winter, however, during S and SW winds their direction may be reversed, and under N wind, an eastwards longshore current occurs (Karditsa 2010). Within the Samothraki Plateau and Lemnos Trough (Figure 1) the so-called 'Samothraki Anticyclone' is formed on a semi-permanent basis, controlling the offshore water circulation and being related to the transport of the Black Sea Water (BSW), which is characterized by low surface salinity and SPM concentration (Zervakis and Georgopoulos 2002). The overall water circulation affects the dispersion of the Evros river plume, by transporting SPM southwards and under the influence of the Samothraki Anticyclonic circulation, combined with the prevailing NE winds (Kokkos and Sylaios 2016).

2.2. Data processing

I*n-situ* water sampling and Inherent Optical Properties (IOPs) data were acquired along transects T1 and T2 (see Figure 1 for locations), simultaneously with a Landsat-8 satellite

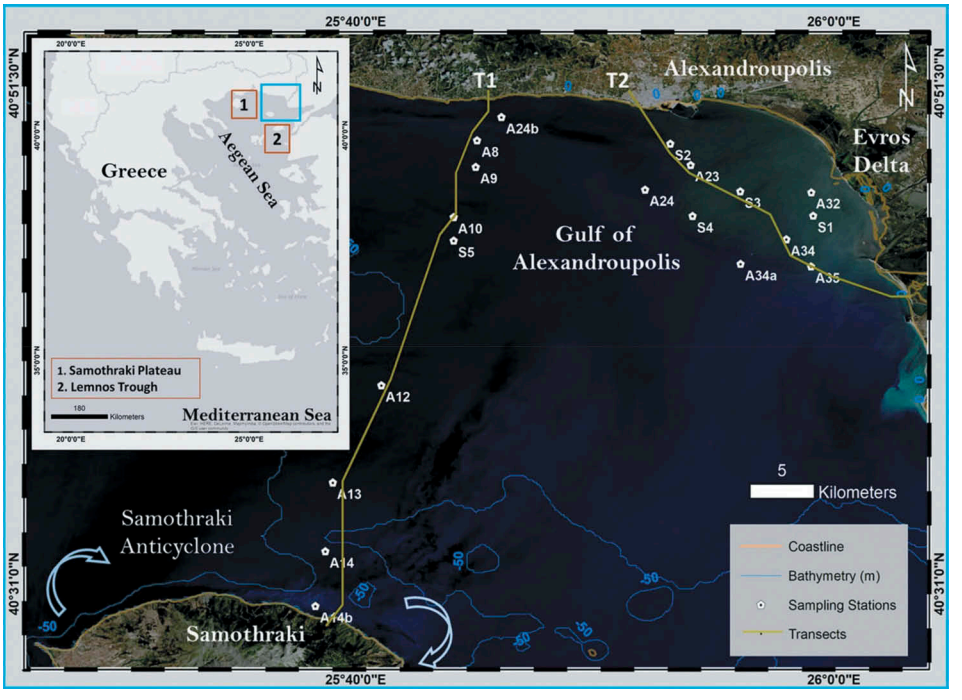

Figure 1. Bathymetry of Alexandroupolis Gulf with the 19 sampling stations on an L8/OLI imagery acquired on 2 June 2016 along with the sampling transects T1 and T2. The main surface circulation pattern of Samothraki's Anticyclone is represented with grey arrows (after Olson et al. 2007). On the upper left corner, the location of survey within Aegean sea, Greece (Eastern Mediterranean sea) is represented. Numbers 1, 2 indicate the Samothraki Plateau and the Lemnos Trough, respectively.

passage over the study area, on 2 June 2016. The field campaign took place under NE prevailing winds of <2 Beaufort speed, with the same conditions recurring 1 week before the sampling (National Observatory of Athens, NOA). Furthermore, the survey was conducted during low river discharge period (i.e. of 22 mg l^{-1} in the river mouth), which remains representative of the sediment loads in the area, since the discharge conditions are subject to slight fluctuations either for almost entirely dammed large rivers (i.e. >10.000 km^2 drainage area; Poulos and Collins 2002), or for medium to small rivers, whose outflows are related to flood events (Skoulikidis et al. 2017). In addition, satellite imagery proved difficult to be collected during such flood events, due to usually heavily cloudy (if not rainy) weather conditions. Table 1 presents the surface distributions statistics along the transects T1 and T2 of the *in-situ* surface parameters (temperature, salinity and density anomaly) within Alexandroupolis Gulf; all the parameters followed a similar surface distribution, with maximum values along T2, being affected by the vicinity of the Evros river mouth and its discharging activity.

2.2.1. Field data

In order to obtain SPM concentrations, seawater samples were collected in bottles of 1.5 Lt volume, at a total of 19 stations along transects T1 and T2 (Figure 1). The water samples underwent laboratory analysis, initially through pre-weighed filters with a pore diameter

Table 1. Minimum, maximum, mean and standard deviation of biogeochemical and optical *in-situ* surface parameters (SPM, temperature, salinity, density anomaly and b_{bp}).

Layer	Parameter	Min	Max	Mean	Standard deviation
Surface (0–2 m)	Temperature (°C)	21.68	24.04	22.87	0.61
	Salinity (psu)	28.7	35.4	33.59	1.93
	Den. An. (Kg m^3)	12.13	24.31	21.56	3.63
	b_{bp} 10^{-3} (m^{-1})	0.0025	0.8763	0.2102	0.26
	SPM (mg l^{-1})	0.32	15.76	4.93	4.43

of 0.2 μm followed by placing the filters in Petri dishes and finally in a desiccator. The filters were weighed repeatedly until a constant weight was obtained on a Mettler Toledo analytical scale of a 10^{-5} g resolution. The SPM was then defined as the ratio of the dry material (in mg) retained on the filters to the sample volume filtered each time. A Sea–Bird Electronics 11plus deck unit CTD (Conductivity, Temperature, Depth) interfaced with a Sea–Bird Electronics 9plus underwater unit, collecting the above information at each station.

Along with the water sampling, *in-situ* remote sensing reflectance (R_{rs}) data were also collected, with above radiance and irradiance measurements. The field recordings of R_{rs} were obtained by using a handheld portable spectroradiometer (Jaz Ocean Optics), in the range between 200 and 890 nm, with a 1.3 nm spectral resolution attached to a 3° FOV Gershun tube via a flexible optical fibre. Surface radiance spectra were taken at every station during the survey. In order to remove the surface reflected light, a small black tube (4.5 cm diameter by 55 cm long) was attached to the front side of the Gershun tube, allowing it to be dipped just below the sea surface (Lee et al. 2010). This technique permits an average of 10 spectra collection, requiring approximately one-minute, whilst the calibration of the radiometer is automated. The remote sensing reflectance is then given as:

$$R_{rs}(0^+) = \frac{L_w(0^+)}{E_d(0^+)} \tag{1}$$

where L_w (0^+) is the seawater leaving radiance and E_d (0^+) is the downwelling irradiance.

The *in-situ* measurements of the backscattering coefficient (b_{bp}) were collected by using the WET-Labs ECO-BB measuring volume scattering function (VSF) at 124° and 650 nm. From the VSF measurements the particle volume scattering, $\beta_p(124°, \lambda)$, can be calculated by subtracting the molecular scattering of seawater (after Morel 1974). The particle backscattering coefficients, b_{bp} (λ) (units of m^{-1}) can then be determined from the single measurement of $\beta_p(124°, \lambda)$ and by using an adjustment X factor according to the water type (Boss and Pegau 2001) :.

$$b_{bp}(\lambda) = 2\pi X \beta_p(124^\circ, \lambda) \tag{2}$$

In the case of the NE Aegean Sea $X = 1.706$, as proposed by Sullivan et al. (2013), convolved with the weighting functions at the centroid angles for the WET Labs ECO BB (124°) sensors. Therefore, the b_{bp} (655) can then be computed:

$$b_{bp}(\lambda) = b_{bp}\left(\frac{\lambda_0}{\lambda}\right)^{\gamma} \tag{3}$$

where $\lambda = 655$ nm, $\lambda_0 = 650$ nm and $\gamma = 1.8$ is the spectral shape exponent, fine-tuned for the North Aegean Sea from reflectivity (Karageorgis et al. 2017) and backscattering field data. The b_{bp} (655) was then used to fit a regression model, calibrated via 19 SPM sampled data.

Regarding spectral reflectance measurements, a regression model was developed by using the *in-situ* SPM observations as the dependent variable and various combinations of the *in-situ* Ocean Optics R_{rs} data as the independent variable, simulated for the L8/OLI bands. Then, the model was applied using the actual L8/OLI bands B2 (480 nm), B3 (560 nm) and B4 (655 nm) satellite data as input (Tsapanou et al. 2018). The predictive accuracy of the newly generated multi-band model was simulated by implementing the Leave-One-Out Cross Validation technique (LOOCV) by Volpe, Silvestri, and Marani (2011); LOOCV produces for each simulation a distribution of the model prediction error that is summarized by its mean and standard deviation. One sample was left out for validation purposes, and the rest were used as training data to fit a regression model, which was then applied to estimate the SPM of the excluded sample. This process was repeated 19 times to predict the SPM at the equivalent 19 stations.

2.2.2. Satellite data

A Level 1T L8 image was retrieved (http://earthexplorer.usgs.gov/) on 2 June 2016 at 08:57 UTC, covering the north-eastern Aegean Sea. L8 carries the Operational Land Imager (OLI) and the Thermal Infrared Sensor (TIRS) with OLI being a push-broom scanner of a 185 km swath and with eight channels at 30 m and one panchromatic channel at 15 m spatial resolution. L8 has a near-polar sun-synchronous orbit at 705 km mean altitude, with a 99-min period and a 16-day revisiting frequency. The image was provided both radiometrically corrected and orthorectified (UTM projection and WGS84 datum) distributed as scaled digital numbers (DN), which can then be converted to calibrated reflectance values and, thus, to SPM concentrations by using OLI B4 (630–680 nm) and B5 (845–885 nm). The image atmospheric correction was processed by the ENvironment for Visualizing Images (ENVI) software (version 5.3) with the built-in tool FLAASH (Fast Line-of-sight Atmospheric Analysis of Hypercubes) (Berk et al. 1999).

To estimate SPM concentration from the satellite image, the methodology proposed by Vanhellemont and Ruddick (2014) was adapted, using the single band algorithm (Nechad, Ruddick, and Park 2010):

$$(\mathrm{SPM}) = \frac{A\rho_w(\lambda)}{1 - \rho_w(\lambda)/C} + B \tag{4}$$

where $A = 289.29$ g m^{-3}, $B = 2.10$ g m^{-3} and $C = 0.1686$ (dimensionless) are the non-linear regression coefficients for L8/OLI B4 (at 655 nm), as indicated in Nechad, Ruddick, and Park (2010). The coefficients A and C are related to IOPs, while B accounts for uncertainties in the measurements. The parameter C is the asymptotic limit of Equation (4) where SPM tends to infinity and it is determined only by the type of particles and not by their concentration (Dogliotti et al. 2015).

The atmospherically corrected product provided the water-leaving reflectance $\rho_w(\lambda)$ in the red band, which can be converted to remote sensing reflectance $R_{rs}(\lambda)$ through the equation (ENVI 2009):.

$$R_{rs}(\lambda) = \frac{\rho_w(\lambda)}{\pi} \quad (5)$$

The single band algorithm was then locally tuned for estimating the L8/OLI derived SPM, by implementing the calibrated model coefficients, developed through a regression fitting in the *in-situ* SPM dataset.

The different SPM retrieval models (*in-situ* b_{bp}, single band (not-tuned), locally tuned, newly generated multi-band) were validated by means of five statistical parameters, providing information on their performance and uncertainty: (i) the coefficient of determination (R^2), indicating the covariance between the *in-situ* measurements and the model-derived SPM; (ii) the average relative percentage error (Bias%); (iii) the Root-Mean-Square Error (RMSE); (iv) the Mean Relative Absolute Difference (MRAD), between the algorithm result and the measurement, weighted against the field SPM; and (v) the average Ratio of estimated to measured data, calculated based on the original values.

3. Results

3.1. Analysis of the cruise measurements

The surface SPM concentrations within the Alexandroupolis Gulf ranged between 0.32 and 15.76 mg l^{-1} during the field survey, on 2 June 2016 (i.e. low load period), with an average concentration of ~5 mg l^{-1}, whereas maximum values appeared close to the coastline, influenced by the Evros river discharge (Table 1). Water surface temperature and salinity varied between 21.5°C and 24.04°C and 28.7–35.4 psu, respectively, proving the presence of both the Evros river and the less saline BSW (Figure 2(a,b)).

Overall, near the Evros mouth (i.e. at the middle of transect T2) high surface SPM concentrations were encountered, forming the Evros plume and being related to high b_{bp} values, but of low Salinity, Temperature and Density (Table 1), indicating its purely riverine origin. Further offshore (at 25–30 km) and westwards (i.e. along transect T1) there is weak presence of the Evros plume identified at the middle of T1 as a local increase of surface SPM and related to low b_{bp} (Figure 2(c,d)).

3.2. Intercomparison and calibration of optical measurements

3.2.1. SPM retrieval model based on in-situ b_{bp} measurements

In Figure 3(a,b), the scatter plots indicate that the *in-situ* surface remote sensing reflectances R_{rs} (i.e. retrieved at the red band) are strongly correlated with both the equivalent b_{bp} (R^2 = 0.88) and the field SPM concentrations (R^2 = 0.87).

In addition, the surface *in-situ* b_{bp} and SPM have a strong correlation of R^2 = 0.94 between them (Figure 4), where a calibrated SPM retrieval model for the entire surface dataset can be expressed in the form of a linear function:.

$$(\mathrm{SPM})_{b_{bp}} = 16.5 \times b_{bp}(655) + 1.44 \quad (6)$$

From the slope of the linear regression established between $b_{bp}(655)$ and SPM, the SPM-specific backscattering coefficient is calculated equal to 0.057 m^{-1} mg l^{-1}, which is slightly higher than the values reported in the literature for coastal waters (Neukermans et al. 2012); this is most probably due to the fact that our dataset is within the Evros river delta,

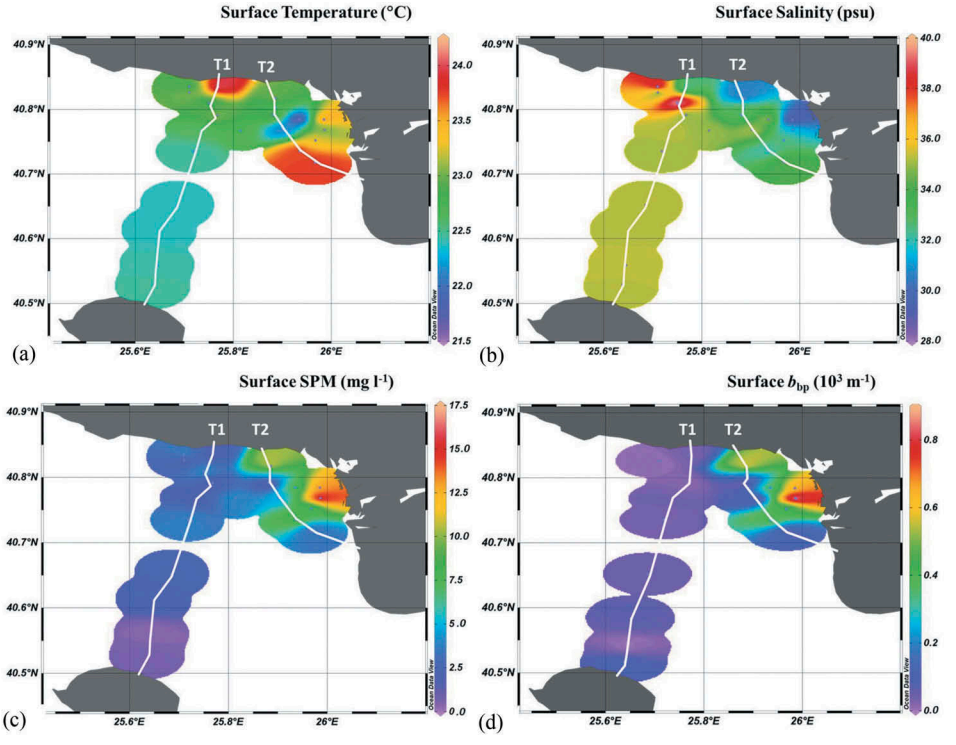

Figure 2. Spatial surface distribution of *in-situ* (a) temperature (°C), (b) Salinity (psu), (c) SPM (mg l^{-1}) and (d) backscattering coefficient (b_{bp}) (10^{-3} m^{-1}) along the transects T1 and T2, on 2 June 2016.

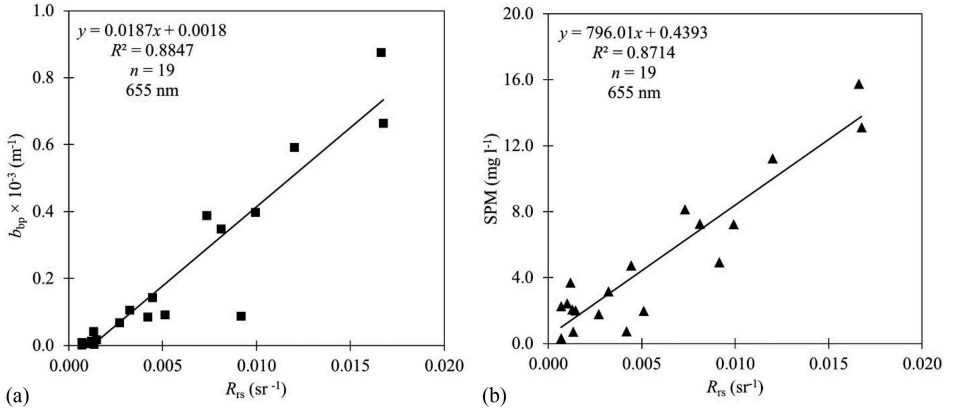

Figure 3. Scatter plots in the Alexandroupolis Gulf during the cruise on 2 June 2016 between *in-situ* surface (a) b_{bp} (at the red band) and R_{rs}, (b) SPM concentrations and R_{rs}.

a zone full of mineral-rich particles. The overall low in both the b_{bp} and SPM values during the survey imply the decreased discharge activity of the Evros river during summer, though even at these conditions there is a strong positive correlation between these two parameters.

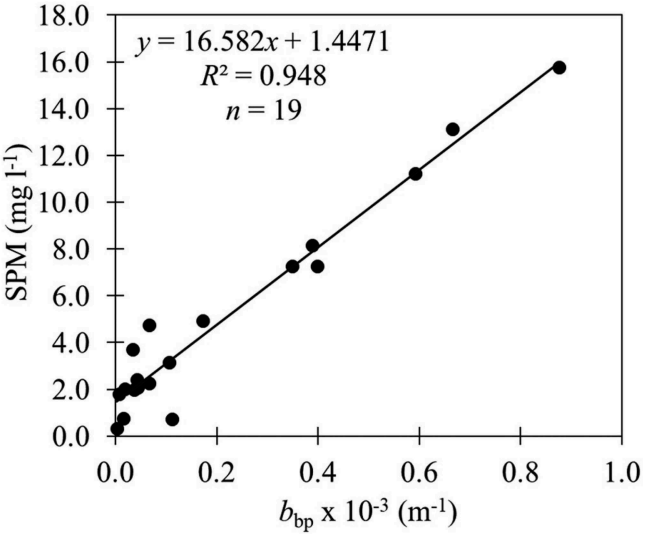

Figure 4. Scatter plot between surface in-situ b_{bp} (at the red band) and SPM concentrations, in the Alexandroupolis Gulf during the cruise on 2 June 2016.

3.2.2. L8/OLI SPM retrieval single band models

In order to obtain satellite-derived SPM concentrations, Nechad's single band model (Equation 4) was applied for L8/OLI and then it was locally tuned specifically for the study area, being expressed by the equation:

$$\mathrm{SPM} = \frac{366.53\rho_w(\lambda)}{1 - \rho_w(\lambda)/0.0324} \tag{7}$$

where $\rho_w(\lambda) = R_{rs}(\lambda)\pi$ and λ is the L8/OLI B4 red band. To avoid the cut-off situation encountered at low SPM range, the offset parameter B of Equation (4) has been removed ($B = 0$).

The application of Nechad's single band (not-tuned) model on the L8/OLI reflectance dataset revealed a fairly good performance in SPM retrieval, although with certain inherent limitations at low SPM concentrations that explain the high Bias value of about 200%. The specific algorithm leads to an over-estimation of SPM at very low concentration, due to the adoption of a constant offset of 2.10 g m^{-3}. Once $\rho_w(655)$ is no greater than 0.03 (a situation frequently encountered in low-turbidity waters), then increased SPM values can be generated. Such very low turbid waters were not considered in the calibration data set used by Nechad, Ruddick, and Park (2010), as their minimum SPM value reached only 1.2 g m^{-3}.

From the comparison of the locally tuned single band model against the surface *in-situ* SPM values at all 19 sampling stations (Figure 5), the statistical analysis indicated that the SPM retrieval model was well tuned for L8/OLI over the study area (MRAD = 89.12%; RMSE = 3.059) and was improved by ~5% compared to the not-tuned version.

3.2.3. Development of a multi-band SPM retrieval model

To compare the satellite-derived surface reflectance against the *in-situ* SPM values, the visible bands of L8/OLI are considered (Figure 6). The satellite reflectance (R_{rs}) increases

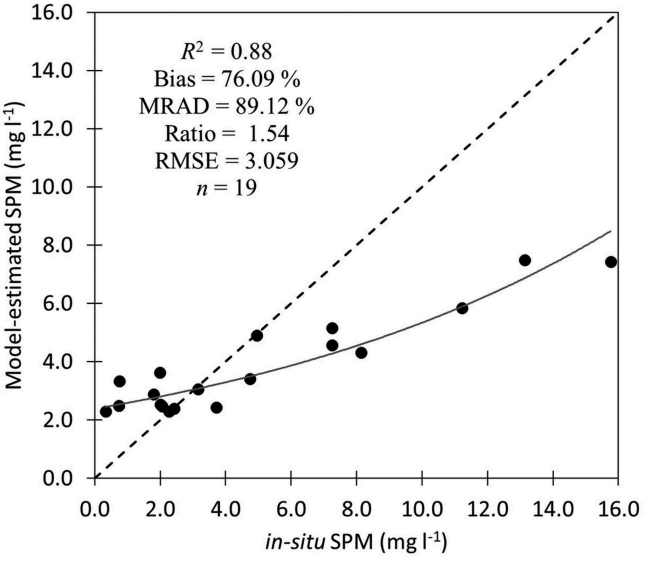

Figure 5. *In-situ* SPM concentrations compared to estimated SPM from the locally tuned single-band model. Dotted-line corresponds to 1:1 line.

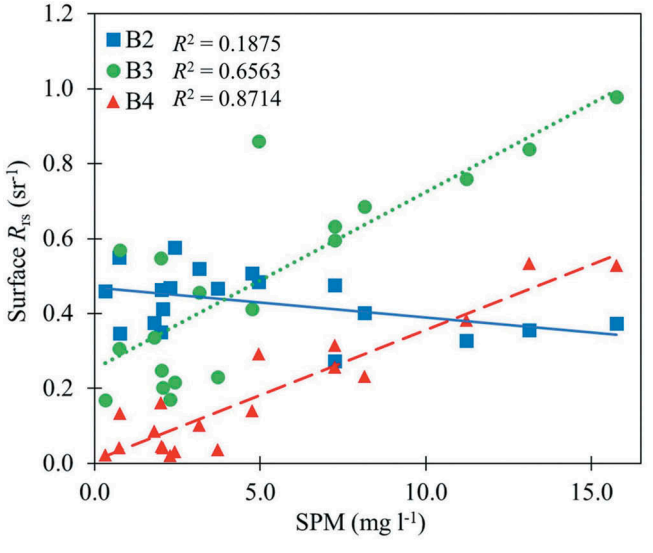

Figure 6. Variation in measured spectral response with increasing SPM, for the visible spectrum of L8/OLI, for bands B2 (Blue) (linear-solid line), B3 (Green) (linear-dotted line) and B4 (Red) (linear-dashed line).

along with SPM for the bands B3 (green) and B4 (Red), whereas R^2 is found 0.65 ($p < 0.005$) and 0.87 ($p < 0.005$), respectively. Nevertheless, for B2 (Blue), there exists a weak (and negative) correlation ($R^2 = 0.18$, $t = -1.98$, $p > 0.005$), confirming that the blue band is neither the most appropriate nor to be considered solely by itself when calibrating and

validating satellite-derived surface reflectance against field observations, particularly in the presence of SPM and next to river mouths.

When considering best fitting for a regression equation in the performance of various visible band combinations, then the *in-situ* SPM has greater R^2 correlation with the square root of the satellite red band, $R_{rs}(655)^2$ (R^2 = 0.87), the red-to-blue band ratio, $R_{rs}(655)/R_{rs}(480)$ (R^2 = 0.82) and the sum of the red and green bands, $R_{rs}(560) + R_{rs}(655)$ (R^2 = 0.76) (Table 2). Especially, when taking the ratio of the square root of the red band to the sum of green and red band, then an overall correlation of R^2 = 0.92 is obtained (Figure 7(a)). Therefore, a multi-band algorithm is derived in the form of the following equation for predicting SPM concentration (mg l^{-1}) from the L8/OLI derived surface reflectance R_{rs}:

$$(\mathrm{SPM})_{R_{rs}(\lambda)} = 5944.3X + 1.41 \tag{8}$$

where $X = \frac{R_{rs}(655)^2}{R_{rs}(560)+R_{rs}(655)}$.

The Leave-One-Out Cross Validation (LOOCV) technique was implemented in the output of the multi-band model and the statistical analysis indicated the model's stability (Table 3). In Figure 7(b) the scatter plot shows a significantly strong correlation (R^2 = 0.93, $p < 0.001$) between the *in-situ* SPM values and the L8/OLI derived SPM estimates taken from Equation (8). For an algorithm in the general linear form of SPM $= aX + \beta$, the null hypothesis was tested; for the intercept being equal to zero it actually resulted into a = 0.708, RMSE = 1.646, and for the slope a being equal to unity we found β = 0.0001, RMSE = 5.567 (Table 4). Therefore, the intercept and slope of the regression line between the measured and the satellite-derived SPM values were slightly different from zero (i.e. t = 0.0001, p = 1.3921e-66) and unity (i.e. t = 0.866, p = 2.0217e-11), respectively, indicating that the combined ratio of the square root red band to the sum of the red and green band obtained an unbiased SPM estimation.

Following the calibration process presented above, a comparison was undertaken by examining the differences (δ) between the satellite-derived atmospherically corrected R_{rs} and the *in-situ* R_{rs} values observed at the 19 surface cruise stations within the study area (Figure 8). Overall, there is a good agreement between the two datasets, however, the simulated satellite products showed greater variation of reflectance with respect to wavelength and location. The R_{rs} differences (δ) ranged between ±0.002 sr^{-1}, but they reached +0.008 sr^{-1} only at stations S5 and A12, implying a strong overestimation from the L8/OLI data; these stations are the farthest away from the coastline where BSW properties dominated.

Table 2. Statistical analysis (determination coefficients (R^2), root-mean-square error (RMSE), *t*, *p*) of the regressions for L8/OLI bands B2 (λ_1-480 nm), B3 (λ_2-560 nm) and B4 (λ_3-655 nm) and for the band-combinations with the best fitting.

λ	Regression equation	R^2	RMSE	t	p
λ_1	$y = -2346.3x + 15.044$	0.18	3.89	−1.98	0.06
λ_2	$y = 1392.1x - 1.8197$	0.65	2.53	5.70	0.00
λ_3	$y = 2499.5x + 0.4393$	0.87	1.55	10.73	0.00
$\lambda_1 + \lambda_2$	$y = 1479.3x - 8.6173$	0.57	2.80	4.84	0.00
$\lambda_1 + \lambda_3$	$y = 2766.7x - 11.964$	0.74	2.19	7.02	0.00
$\lambda_2 + \lambda_3$	$y = 928.3x - 1.2387$	0.76	2.11	7.36	0.00
λ_2/λ_3	$y = 8.3149x + 0.9796$	0.82	1.80	8.98	0.00
$(\lambda_1 + \lambda_2)^2$	$y = 60867x + 1.2392$	0.84	1.76	9.22	0.00
$(\lambda_3^2)/(\lambda_2 + \lambda_3)$	$y = 5944.3x + 1.41$	0.92	1.17	14.54	0.00

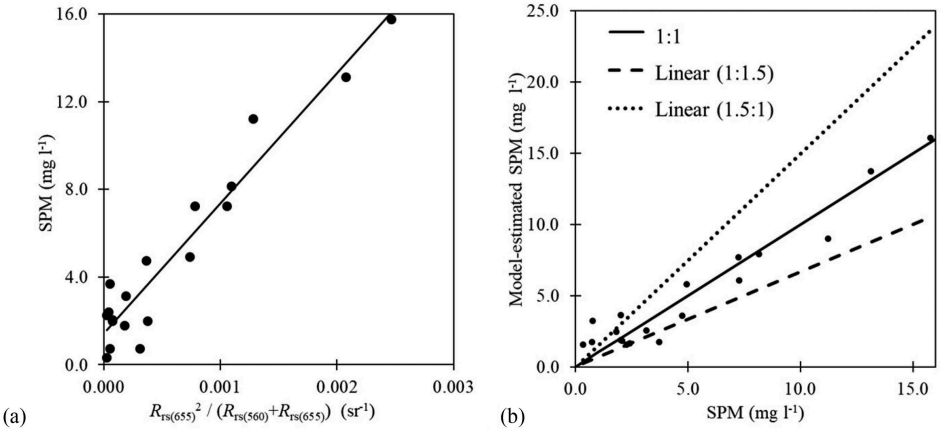

Figure 7. (a) Regression model between *in-situ* SPM concentrations and the combination of the L8/OLI reflectances, $R_{rs,}$ (square root red band divided by the sum of green and red band); (b) Scatter plot between *in-situ* SPM concentration values and those derived from the multi-band model.

Table 3. Statistics of the original (not-tuned) Nechad's model, its locally tuned version and the new-generated multi-band model.

Model Reference	R^2	Bias (%)	RMSE	MRAD	average Ratio (estimated to measured value)
Nechad's model (not-tuned)	0.82	200.42	2.99	2.08	3.00
Locally-tuned Nechad's model	0.88	76.09	3.05	0.89	1.54
Multi-band model	0.92	40.60	1.17	0.63	1.40

Table 4. Statistics of 19 exponential models for the L8/OLI bands B2, B3, B4 for validating the best-fitting L8/OLI satellite-derived SPM estimation using the leave-one-out cross validation (LOOCV) technique (SPM $= aX + \beta$, from Equation (8)).

	α	β	R^2	RMSE
Maximum	0.7218	3.8046	0.9551	1.4192
Minimum	0.6107	3.3670	0.8014	0.7302
Mean	0.7016	3.5499	0.9262	0.8917
Std. Dev.	0.0271	0.1026	0.0315	0.1304

Comparing the remotely sensed R_{rs} derived from the L8/OLI imagery by using the three algorithms, the single band model showed a regression coefficient of $R^2 = 0.82$, whereas its tuned version generated SPM retrievals within a 91% agreement with the *in-situ* measurements, corresponding to a regression coefficient of $R^2 = 0.83$ and an RMSE of 3.5 (Figure 9(a)). On the other hand, the multi-band algorithm efficiency showed an improved 96%-agreement with the *in-situ* SPM measurements ($R^2 = 0.93$).

4. Discussion

The quantitative evaluation of reflectances, $R_{rs,}$ suggested that there is an average of ~20% overestimation in most of the L8/OLI channels compared with the *in-situ* observations. In addition, at the offshore locations the L8/OLI-derived R_{rs} at B1 (480 nm) seemed to be closer

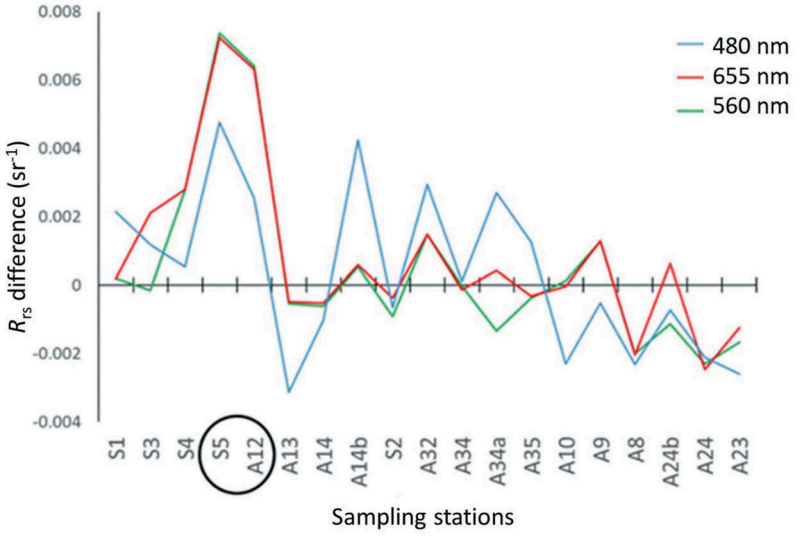

Figure 8. Difference (δ) of R_{rs} values between the L8/OLI-derived R_{rs} and the spectrally resampled *in-situ* R_{rs} along the survey site, at 480 nm, 560 nm and 655 nm. In the black circle, the two offshore stations S5 and A12 are included.

to the *in-situ* data compared to the R_{rs} derived from B3 (560 nm) and B4 (655 nm), whereas at all other locations this situation reversed. The L8/OLI data tended consistently to slightly underestimate R_{rs} at stations along the north-western coastal part of the Alexandroupolis Gulf, regardless whether the actual SPM concentrations were either high (Stations A23 and S2) or low (Stations A8, A24 and A24b). These errors may occur due to the shape and the intensity of the reflectance spectrum, as suggested by Novo, Hansom, and Curran (1989).

Based on the surface reflectance R_{rs} retrieved from the L8/OLI band combinations, we developed a multi-band satellite-derived SPM algorithm, which showed a better fit with *in-situ* measurements, compared to the original Nechad's model and its locally tuned version. Having included the green band (560 nm), the newly generated algorithm seemed to create more accurate SPM estimations than Nechad's single band formulas that are based only on the red channel (655 nm) reflectance (Figure 9(a)). This result could be partly due to the fact that single band algorithms are highly sensitive to atmospheric scattering and, consequently, they are subject to uncertainties; on the other hand, the band ratio algorithms can largely cancel the background scattering effects and reduce the error range. For high reflectance values, the relationship between R_{rs} – SPM becomes non-linear and reflectance approaches asymptotically the maximum 'saturation' value (Bowers, Boudjelas, and Harker 1998), whereas increased suspended sediment concentrations no longer affect the reflectance. By assuming that particle scattering and absorption are proportional to SPM, in Nechad's singe band algorithm it is observed that at low reflectance values (<0.02) this relationship is almost linear, before reaching to an asymptotic value (near 0.03). Thus, the single band models perform better at low reflectance values, while their accuracy depends on the proportionality of backscattering with SPM. In addition, all empirical algorithms are subject to uncertainties induced by the failure of matching the materials that contribute to R_{rs} and those that dominate SPM; for example,

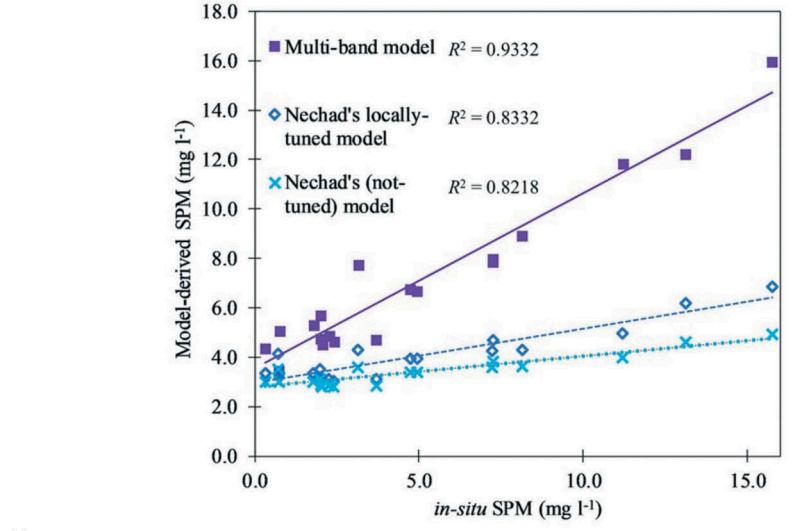

(a)

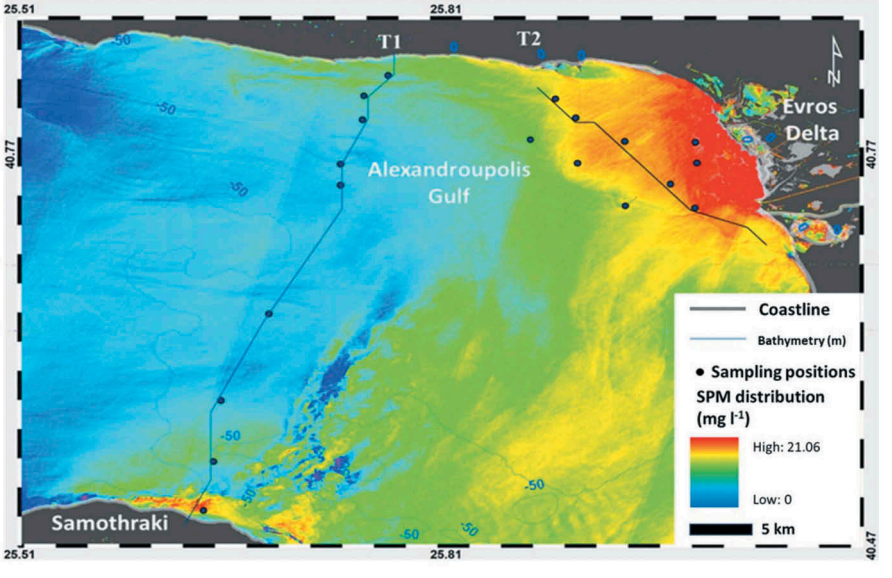

(b)

Figure 9. (a) Scatter plots showing the linear relationship between *in-situ* surface SPM and satellite-derived SPM when applying Nechad's (not-tuned) algorithm (big dashed line), Nechad's locally tuned algorithm (small dashed line) and the new-generated multi-band algorithm (solid line), using L8/OLI derived surface reflectance R_{rs}. (b) The L8/OLI derived SPM distribution map on 2 June 2016, after applying the developed multi-band algorithm.

Coloured Dissolved Organic Matter (CDOM) may reduce R_{rs} depending on the wavelength λ, however, it is irrelevant for SPM estimations (Zheng and DiGiacomo 2017).

The biogeochemical and optical *in-situ* surface parameters along with the *in-situ* surface SPM, indicate similarities with previous studies by showing that this part of the continental

shelf has a year-round very low turbidity, especially during the reduced discharge period of the Evros river (Kanellopoulos et al. 2009). Equally, important is to take into account the temperature and salinity dependency, when the red band is involved for deriving water quality parameters. More specifically, the upper surface layer's salinity, temperature and density remained unchanged, implying that extensive mixing has been taken place offshore, between the river waters and the BSW. The backscattering coefficient, $b_{bp,}$ and the *in-situ* SPM measurements showed a good correlation, proving that b_{bp} is an appropriate proxy for studying sediment dynamics in coastal areas, where inorganic matter dominates.

Differences in sediment composition and grain size distribution may also influence the optical properties of the aquatic environment (Lodhi et al. 1997). Therefore, in the red spectrum (i.e. 655 nm), the attenuation coefficient due to particles, $c_{p,}$ may also be used as an alternative proxy to backscattering; this coefficient is controlled by particle absorption and scattering properties, since absorption by CDOM is minimal (Morel and Loisel. 1998).

The satellite-derived SPM distribution within the Alexandroupolis Gulf is assumed not to be affected by bathymetry, since this investigation has taken place at water depths >10 m, with only a few stations being located between 5 and 10 m, where the seafloor's influence is supposed minimal. Nevertheless, additional measurements of the absorption coefficients may improve potential errors in the SPM estimations, since higher concentrations may occur, especially in wet season or during flood events (Kanellopoulos et al. 2009).

Exploitation of other satellites than Landsat (e.g. Sentinel-2, MODIS, etc.) and under different spatio-temporal resolution can also monitor larger sediment loads associated with flooding events, which usually are related to long periods of cloudiness that restrict satellite imaging; the imminent high sediment loads during flooding can be also encountered if implementing innovative modelling processes based on precipitation, stream gauges, etc. Therefore, more field surveys during periods of high and low concentrations are required to reveal a larger dynamic SPM range for algorithm application.

Figure 9(b) presents a map of the L8/OLI-derived SPM distribution within the entire study area for 2 June 2016, computed from the newly developed algorithm and revealing insights into several interesting formations at small spatial scales. As expected, there was a maximum SPM concentration in the proximity of the Evros river mouth (i.e. about 5 km offshore), though the absolute values were low given the river's decreased discharge. The surface high SPM Evros plume seemed to be restricted and directed mainly southwards from the river mouth; a movement that was further enhanced by northerly winds prevailing during the last few days and during the field cruise. The influence of the Evros SPM output extended south-southeast at >40 km from the river mouth, where the Dardanelles outflow prevails. The Evros plume did not seem to propagate westwards, possibly inhibited by the Samothraki anticyclone. Hence, high SPM values found along the northern coast of the Samothraki island, could be related to other local processes, such as strong thermal spring discharge and sediment resuspension. Other explanation to these changing patterns of SPM distribution, may be related to the different ocean dynamics during sampling (tide, waves, wind, current, etc.), regardless the fact that during the investigation no wave activity existed, with wind being of <2 Beaufort; for instance, according to the seasonal hydrological features (i.e. Coriolis force movement), spatial modulation of SPM is induced, by settling the riverine material in the Alexandroupolis Gulf, or by transferring it even 100 km away from Evros mouth (Kanellopoulos et al. 2008).

5. Conclusions

In the Alexandroupolis Gulf, located in the NE Aegean Sea and being influenced by the Evros river, L8/OLI remotely sensed ocean colour and field data implied a strong correlation between the particle backscattering coefficient and the SPM concentrations. Subsequently, a single band model for SPM retrieval was tested and calibrated with *in-situ* R_{rs} measurements and a multi-band algorithm was developed. The SPM was calculated from the new-generated retrieval model, after been validated with the LOOCV method, showing that the L8/OLI can generate reasonably good R_{rs}, which result in quantifying SPM distribution and variation within the Alexandroupolis Gulf. The proposed SPM satellite-retrieval algorithm seemed to provide improved results when compared to published empirical models, though it remained sensitive to surface dynamics, therefore requiring further appropriate tuning according to surface water biochemical properties.

Future work may include determining the SPM distribution on a larger spatio-temporal scale, associated with a wider range of SPM concentrations and by using satellite data based on the model developed, calibrated and validated in this study. In addition, a quality check can be provided on different satellite data (i.e. Sentinel-2) by conducting inter-sensor comparisons. The satellite-derived SPM estimations can then be combined with available hydrodynamic information and circulation modelling for SPM monitoring even during flooding events and cloudy skies.

Acknowledgements

This work was supported by the Greek National Scholarships Foundation '(IKY)' research fellowship under Grant c.n. 2017-050-0504-10421, which was funded by the Act 'Scholarship program for postgraduate studies; second circle', from resources of the Operational Program 'Human Resources Development, Education and Lifelong Learning' 2014–2020 with the co-funding of the European Social Fund and the Hellenic State.

Disclosure statement

No potential conflict of interest was reported by the authors.

Funding

This work was supported by the Greek National Scholarship Foundation [c.n. 2017-050-0504-10421].

References

Alcântara, E., M. Curtarelli, and J. Stech. 2016. "Estimating Total Suspended Matter Using the Particle Backscattering Coefficient: Results from the Itumbiara Hydroelectric Reservoir (Goiás State, brazil)." *Remote Sensing Letters* 7 (4): 397–406. doi:10.1080/2150704X.2015.1137646.

Berk,A. G. P. A., G. P. Anderson, P. K. Acharya, J. H. Chetwynd, L. S. Bernstein, E. P. Shettle, and S. M. Adler-Golden. 1999. "MODTRAN4 user's manual." *Air Force Research Laboratory* 1.

Boss, E., and W. S. Pegau. 2001. "Relationship of Light Scattering at an Angle in the Backward Direction to the Backscattering Coefficient." *Applied Optics* 40: 5503–5507. doi:10.1364/AO.40.005503.

Bowers, D. G., S. Boudjelas, and G. E. L. Harker. 1998. "The Distribution of Fine Suspended Sediments in the Surface Waters of the Irish Sea and Its Relation to Tidal Stirring." *International Journal of Remote Sensing* 19 (14): 2789–2805. doi:10.1080/014311698214514.

Dogliotti, A. I., K. G. Ruddick, B. Nechad, D. Doxaran, and E. Knaeps. 2015. "A Single Al- Gorithm Be Used to Retrieve Turbidity from Remotely-sensed Data in All Coastal and Estuarine Waters." *Remote Sensing of Environment* 156: 157–168. doi:10.1016/j.rse.2014.09.020.

Doxaran, D., J. M. Froidefond, and P. Castaing. 2002b. "A Reflectance Band Ratio Used to Estimate Suspended Matter Concentrations in Sediment-Dominated Coastal Waters." *International Journal of Remote Sensing* 23 (23): 5079–5085. doi:10.1080/0143116021000009912.

Doxaran, D., J. M. Froidefond, S. Lavender, and P. Castaing. 2002a. "Spectral Signature of Highly Turbid Waters: Application with SPOT Data to Quantify Suspended Particulate Matter Concentrations." *Remote Sensing of Environment* 81 (1): 149–161. doi:10.1016/S0034-4257(01)00341-8.

ENVI. 2009. "ENVI Atmospheric Correction Module: QUAC and FLAASH User's Guide." *Module Version*.

Froidefond, J. M., L. Gardel, D. Guiral, M. Parra, and J. F. Ternon. 2002. "Spectral Remote Sensing Reflectances of Coastal Waters in French Guiana under the Amazon Influence." *Remote Sensing of Environment* 80 (2): 225–232. doi:10.1016/S0034-4257(01)00301-7.

Kanellopoulos, T. D., M. O. Angelidis, D. Georgopoulos, and A. P. Karageorgis. 2009. "Fate of the Evros River Suspended Particulate Matter in the Northern Aegean Sea." *Environmental Geology* 57 (8): 1729–1738. doi:10.1007/s00254-008-1454-2.

Kanellopoulos, T. D., V. Kapsimalis, S. E. Poulos, M. O. Angelidis, A. P. Karageorgis, and K. Pavlopoulos. 2008. "The Influence of the Evros River on the Recent Sedimentation of the Inner Shelf of the NE Aegean Sea." *Environmental Geology* 53 (7): 1455–1464. doi:10.1007/s00254-007-0754-2.

Karageorgis, A. P., P. G. Drakopoulos, S. Psarra, K. Pagou, E. Krasakopoulou, A. C. Banks, D. Velaoras, N. Spyridakis, and E. Papathanassiou. 2017. "Particle Characterization and Composition in the NE Aegean Sea: Combining Optical Methods and Biogeochemical Parameters." *Continental Shelf Research* 149: 96–111. doi:10.1016/j.csr.2017.03.008.

Karditsa, A. 2010. "Recent Sedimentation Processes in the Inner Continental Shelf of Alexandroupolis Gulf (North East Aegean sea)." Unpublished PhD Thesis, National and Kapodistrian University of Athens.

Karditsa, A., A. Tsapanou, and S. E. Poulos. 2019. "The Evolution of the Transboundary Evros River Delta (Northeast Aegean sea) under Human Intervention: A Seven-decade Analysis." *Physical Geography* 1–24. doi:10.1080/02723646.2019.1666564.

Karditsa, A., and S. E. Poulos. 2013. "Sedimentological Investigations in a River-Influenced Tideless Coastal Embayment: The Case of Inner Continental Shelf of the NE Aegean Sea." *Continental Shelf Research* 55: 86–96. doi:10.1016/j.csr.2013.01.014.

Kokkos, N., and G. Sylaios. 2016. "Modeling the Buoyancy-Driven Black Sea Water Outflow into the North Aegean Sea." *Oceanologia* 58 (2): 103–116. doi:10.1016/j.oceano.2015.12.003.

Lee, Z. P., Y. H. Ahn, C. Mobley, and R. Arnone. 2010. "Removal of Surface-Reflected Light for the Measurement of Remote-Sensing Reflectance from an above-Surface Platform." *Optics Express* 18 (25): 26313–26324. doi:10.1364/OE.18.026313.

Lodhi, M. A., D. C. Rundquist, L. Han, and M. S. Kuzila. 1997. "The Potential for Remote Sensing of Loess Soils Suspended in Surface Waters." *Journal of the American Water Resources Association* 33 (1): 111–117. doi:10.1111/j.1752-1688.1997.tb04087.x.

Lymburner, L., E. Botha, E. Hestir, J. Anstee, S. Sagar, A. Dekker, and T. Malthus. 2016. "Landsat 8: Providing Continuity and Increased Precision for Measuring Multi-Decadal Time Series of Total Suspended Matter." *Remote Sensing of Environment* 185: 108–118. doi:10.1016/j.rse.2016.04.011.

Meade, R. H. 1996. "River-Sediment Inputs to Major Deltas." In *Sea Level-Rise and Coastal Subsidence* 63–85. Dordrecht: Springer. doi:10.1007/978-94-015-8719-8_4.

Milliman, J. D., and K. L. Farnsworth. 2011. *River Discharge to the Coastal Ocean. A Global Synthesis*. New York: Cambridge University Press.

Moore, G. F., J. Aiken, and S. J. Lavender. 1999. "The Atmospheric Correction of Water Colour and the Quantitative Retrieval of Suspended Particulate Matter in case II Waters: Application to MERIS." *International Journal of Remote Sensing* 20 (9): 1713–1733. doi:10.1080/014311699212434.

Morel, A. 1974. "Optical Properties of Pure Water and Pure Sea Water." *Optical Aspects of Oceanography* 1 (1): 1–24.

Morel, A., and H. Loisel. 1998. "Apparent Optical Properties of Oceanic Water: Dependence on the Molecular Scattering Contribution." *Applied Optics* 37 (21): 4765–4776. doi:10.1364/AO.37.004765.

Nechad, B., K. G. Ruddick, and Y. Park. 2010. "Calibration and Validation of a Generic Multisensor Algorithm for Mapping of Total Suspended Matter in Turbid Waters." *Remote Sensing of Environment* 114 (4): 854–866. doi:10.1016/j.rse.2009.11.022.

Neukermans, G., H. Loisel, X. Meriaux, R. Astoreca, and D. Mc-Kee. 2012. "In Situ Variability of Mass-specific Beam Attenuation and Backscattering of Marine Particles with respect to Particlesize, Density, and Composition." *Limnology and Oceanography* 57 (1): 124–144. doi:10.4319/lo.2012.57.1.0124.

Novo, E. M., J. D. Hansom, and P. J. Curran. 1989. "The Effect of Viewing Geometry and Wavelength on the Relationship between Reflectance and Suspended Sediment Concentration." *International Journal of Remote Sensing* 10 (8): 1357–1372. doi:10.1080/01431168908903973.

Olson, D. B., V. H. Kourafalou, W. E. Johns, G. Samuels, and M. Veneziani. 2007. "Aegean Surface Circulation from a Satellite-Tracked Drifter Array." *Journal of Physical Oceanography* 37 (7): 1898–1917. doi:10.1175/JPO3028.1.

Ouillon, S., P. Douillet, and S. Andréfouët. 2004. "Coupling Satellite Data with in Situ Measurements and Numerical Modeling to Study Fine Suspended-Sediment Transport: A Study for the Lagoon of New Caledonia." *Coral Reefs (Online)* 23 (1): 109–122. doi:10.1007/s00338-003-0352-z.

Poulos, S. E., and M. B. Collins. 2002. "Fluviatile Sediment Fluxes to the Mediterranean Sea: A Quantitative Approach and the Influence of Dams." *Geological Society, London, Special Publications* 191 (1): 227–245. doi:10.1144/GSL.SP.2002.191.01.16.

Qiu, Z. 2013. "A Simple Optical Model to Estimate Suspended Particulate Matter in Yellow River Estuary." *Optics Express* 21 (23): 27891–27904. doi:10.1364/OE.21.027891.

Qiu, Z., C. Xiao, W. Perrie, D. Sun, S. Wang, H. Shen, D. Yang, and Y. He. 2017. "Using Landsat 8 Data to Estimate Suspended Particulate Matter in the Yellow River Estuary." *Journal of Geophysical Research: Oceans* 122 (1): 276–290. doi:10.1002/2016JC012412.

Siswanto, E., J. Tang, H. Yamaguchi, Y. H. Ahn, J. Ishizaka, S. Yoo, and S. W. Kim. 2011. "Empirical Ocean-Color Algorithms to Retrieve Chlorophyll-a, Total Suspended Matter, and Colored Dissolved Organic Matter Absorption Coefficient in the Yellow and East China Seas." *Journal of Oceanography* 67 (5): 627–650. doi:10.1007/s10872-011-0062-z.

Skoulikidis, N. 2018. "The State and Origin of River Water Composition in Greece." *Handbook of Environmental Chemistry* 97–127. doi:10.1007/698_2016_468.

Skoulikidis, N. T., S. Sabater, T. Datry, M. M. Morais, A. Buffagni, G. Dörflinger, and S. Zogaris. 2017. "Non-Perennial Mediterranean Rivers in Europe: Status, Pressures, and Challenges for Research and Management." *Science of the Total Environment* 577: 1–18. doi:10.1016/j.scitotenv.2016.10.147.

Stramski, D., E. Boss, D. Bogucki, and K. J. Voss. 2004. "The Role of Seawater Constituents in Light Backscattering in the Ocean." *Progress in Oceanography* 61 (1): 27–56. doi:10.1016/j.pocean.2004.07.001.

Sullivan, J. M., M. S. Twardowski, J. Ronald, V. Zaneveld, and C. C. Moore. 2013. "Measuring Optical Backscattering in Water." In *Light Scattering Reviews 7: Radiative Transfer and Optical Properties of Atmosphere and Underlying Surface*, 189–224. Springer, Berlin: Heidelberg. doi:10.1007/978-3-642-21907-8_6.

Tassan, S. 1994. "Local Algorithms Using SeaWiFS Data for the Retrieval of Phytoplankton, Pigments, Suspended Sediment, and Yellow Substance in Coastal Waters." *Applied Optics* 33 (12): 2369–2378. doi:10.1364/AO.33.002369.

Tsapanou, A., E. Oikonomou, S. Poulos, and P. Drakopoulos. 2018. "Evaluating Ocean-Color Algorithms to Remotely Sense the Surface Suspended Particle Matter in the Northeast Aegean Sea, Greece." *Proceedings of SPIE - the International Society for Optical Engineering* 10773. doi:10.1117/12.2326133.

Tsimplis, M. N. 1994. "Tidal Oscillations in the Aegean and Ionian Seas." *Estuarine, Coastal and Shelf Science* 39 (2): 201–208. doi:10.1006/ecss.1994.1058.

Vanhellemont, Q., and K. Ruddick. 2014. "Turbid Wakes Associated with Offshore Wind Turbines Observed with Landsat 8." *Remote Sensing of Environment* 145: 105–115. doi:10.1016/j.rse.2014.01.009.

Vantrepotte, V., E. Gensac, H. Loisel, A. Gardel, D. Dessailly, and X. Mériaux. 2013. "Satellite Assessment of the Coupling between in Water Suspended Particulate Matter and Mud Banks Dynamics over the French Guiana Coastal Domain." *Journal of South American Earth Sciences* 44: 25–34. doi:10.1016/j.jsames.2012.11.008.

Volpe, V., S. Silvestri, and M. Marani. 2011. "Remote Sensing Retrieval of Suspended Sediment Concentration in Shallow Waters." *Remote Sensing of Environment* 115 (1): 44–54. doi:10.1016/j.rse.2010.07.013.

Wang, C., S. Chen, D. Li, D. Wang, W. Liu, and J. Yang. 2017. "A Landsat-Based Model for Retrieving Total Suspended Solids Concentration of Estuaries and Coasts in China." *Geoscientific Model Development* 10 (12): 4347–4365. doi:10.5194/gmd-10-4347-2017.

Wiering, M., J. Verwijmeren, K. Lulofs, and C. Feld. 2010. "Experiences in Regional Cross Border Co-Operation in River Management. Comparing Three Cases at the Dutch-German Border." *Water Resources Management* 24 (11): 2647–2672. doi:10.1007/s11269-009-9572-5.

Zervakis, V., and D. Georgopoulos. 2002. "Hydrology and Circulation in the North Aegean (Eastern Mediterranean) Throughout 1997 and 1998." *Mediterranean Marine Science*. doi:10.12681/mms.254.

Zhang, M., J. Tang, Q. Dong, Q. T. Song, and J. Ding. 2010. "Retrieval of Total Suspended Matter Concentration in the Yellow and East China Seas from MODIS Imagery." *Remote Sensing of Environment* 114 (2): 392–403. doi:10.1016/j.rse.2009.09.016.

Zheng, G., and P. M. DiGiacomo. 2017. "Uncertainties and Applications of Satellite-Derived Coastal Water Quality Products." *Progress in Oceanography* 159: 45–72. doi:10.1016/j.pocean.2017.08.007.